Journal of Environmental Management 337 (2023) 117746

Contents lists available at ScienceDirect

Journal of Environmental Management

journal homepage: www.elsevier.com/locate/jenvman

Research article

Computational fluid dynamics modeling of floating treatment wetland retrofitted stormwater pond: Investigation on design configurations

Md Nuruzzaman *, A.H.M. Faisal Anwar, Ranjan Sarukkalige

School of Civil and Mechanical Engineering, Curtin University, GPO Box U1987, Perth, WA 6845, Australia

ARTICLE INFO

Keywords:
Floating wetland
Design
Computational fluid dynamics
Hydraulics
Stormwater management

ABSTRACT

Floating Treatment Wetland (FTW) is a cost-effective and easy-to-retrofit device for stormwater treatment. Its treatment efficiency largely depends on the fraction of inflow entering FTW and the residence time within it. Thus hydrodynamics play a crucial role, which is affected by the design configurations of FTW and stormwater pond. Despite a spike in research on FTWs, very little is known about how various design configurations affect treatment efficiency by an FTW. Our study hypothesizes that relative positions of FTW geometry, FTW position and pond inlet–outlet have impact on the hydrodynamics and as a consequence, treatment efficiency. To explore these design features, we employed computational fluid dynamics (CFD) modeling conducted in ANSYS Fluent, validated by experimental data to examine the impact of the aforementioned design features. The results revealed that circular FTW geometry positioned near inlet coupled with center inlet–side outlet configuration achieved the highest removal (94.8%) for a non-dimensional removal rate of $k_r t_{HRT} = 20$ (k_r is the first order removal rate in per day, t_{HRT} is the nominal hydraulic residence time of the pond in days). Far side inlet–side outlet configuration performed the worst due to profound promotion of short-circuiting. FTW positioned near inlet performed better (61.8% mass removal on an average) than center (42.7%) and near outlet positions (54.1%) for $k_r t_{HRT} = 20$. Sensitivity analysis revealed that the treatment efficiency is most sensitive to inlet–outlet configurations. The design implications of this study will help practitioners achieving better water quality and ecological improvement goals.

1. Introduction

Floating Treatment Wetlands (FTWs) are recently adopted widely for stormwater treatment due to their low cost, effectiveness, capability to operate in variable water depth and easy-to-retrofit characteristics (Colares et al., 2020; Li and Katul, 2020). An FTW consists of a floating bed planted with water-tolerant species, where roots go directly into the water column (Schwammberger et al., 2019). Pollutants in stormwater, e.g., nitrogens, phosphorus, heavy metals are uptaken by plant roots to sustain plant growth. Plant roots provide a large surface area for the microbial population, which helps remove an additional amount of pollutants and increase the bioavailable fraction of pollutants to the plant (Lynch et al., 2015; Winston et al., 2013). Plant roots also trap sediments and particulate pollutants in the root matrix (Borne et al., 2013). As such, plant roots are crucial in achieving higher treatment efficiency by an FTW. However, an FTW will be ineffective if the flowing water does not come in contact with the FTW root zone before exiting the stormwater pond (Lucke et al., 2019). This phenomenon of flowing water bypassing an FTW and exiting the pond with little to no contact with the FTW is known as flow short-circuiting (Khan et al., 2013a). Thus, flow short-circuiting can reduce the treatment efficiency of an FTW. The level of flow short-circuiting can be measured by conducting tracer experiments and calculating different hydraulic performance indices from the residence time distribution (RTD) curve derived through the experiment (Farjood et al., 2015; Lightbody et al., 2009). Hydraulic performance indices can indicate the degree of short-circuiting, mixing and presence of dead zones within the pond.

Previously, only a few studies investigated the factors that influence the hydraulic performance of an FTW retrofitted stormwater pond. Bu and Xu (2013) measured the hydraulic performance of four identical FTW units planted with different species. It was concluded that the hydraulic performance of identical units with different plant species differed significantly, possibly due to the different lengths and volumes of solid roots. No design configurations of the FTW and pond were investigated in this study. Khan et al. (2013a) studied how inlet arrangements, FTW position, orientation and arrangements (single vs

* Corresponding author.
E-mail address: md.nuruzzaman1@postgrad.curtin.edu.au (M. Nuruzzaman).

https://doi.org/10.1016/j.jenvman.2023.117746
Received 5 September 2022; Received in revised form 5 January 2023; Accepted 13 March 2023
Available online 21 March 2023

multiple) impacted the hydraulic performance of an FTW retrofitted pond. Khan et al. (2013a) demonstrated how introducing multiple inlets instead of a single inlet could enhance hydraulic performance. It was also reported that positioning the FTW in the optimum location and orientating the FTW in the right direction can improve hydraulic performance. Conversely, it was depicted that unnecessarily splitting the FTW into multiple FTWs and arranging them in series did not ameliorate hydraulic performance of the pond. Xavier et al. (2018) confirmed the findings of Khan et al. (2013a) that multiple FTWs in series did not provide any additional benefit by estimating nutrient removal through numerical simulation. Xavier et al. (2018) examined nutrient removal performance of multiple FTWs in parallel and reported improvement compared to a single FTW or multiple FTWs in series by computational fluid dynamics (CFD) simulations. Khan et al. (2019) investigated a few more design configurations such as vegetation density (number of plants per unit area) as well as its spatial distribution and submergence depth ratio (ratio of root length to flow depth) by tracer experiments. Even though a number of design configurations were explored in terms of hydraulic performance by Khan et al. (2013a) and Khan et al. (2019), the potential for pollutant mass removal by those design configurations was not quantified by the corresponding studies.

Nuruzzaman et al. (2021) identified a few more design configurations, e.g., inlet–outlet configuration and FTW geometry that have not been investigated to date. It was also mentioned that the FTW position may not always be exploitable due to water depth limitations, as FTWs need a permanent pool of water throughout the year. A minimum distance between the benthic layer and root zone should be maintained to prevent roots from attaching to the bottom, which may not be possible in all parts of the pond (Headley and Tanner, 2012). In this case, modifying the relative positions of inlet and outlet may offer improvement in hydraulic performance and pollutant mass removal. Khan et al. (2013a) studied the impact of inlet positions and arrangements in terms of hydraulic performance as mentioned earlier, but the effect of outlet position was not studied and the pollutant mass removal potential was not quantified for both inlet and outlet variations. Changing an inlet position may force the inflow to pass through the FTW. However, changing the position of outlet has a potential for water recirculation, which can enhance the residence time within FTW and achieve better treatment efficiency. As such, it is crucial to examine the effect of both inlet and outlet position on the pond flow field and treatment efficiency of FTW. In some cases, modifying the positions of inlet and outlet may become costly. In those cases, different geometries of FTW can be utilized to achieve greater hydraulic performance and higher treatment efficiency. Various geometries of FTWs (rectangular, circular, hexagonal, kidney, L-shaped and irregular) have been used in different field-scale studies (Chang et al., 2013; Chua et al., 2012; Faulwetter et al., 2011; Hartshorn et al., 2016; McAndrew et al., 2016; Winston et al., 2013), but the benefits or demerits of different FTW geometries have not been studied in terms of hydraulics, which in turn would affect pollutant removal efficiency.

Lucke et al. (2019) reported that a careful design of FTWs can enhance the treatment efficiency of an FTW through improved hydraulic conditions. Thus the aim of this study is to investigate the impact of the design configurations, e.g., inlet–outlet configuration, FTW position and FTW geometry on the hydraulic performance, flow field of stormwater pond and pollutant mass removal to facilitate better design options for practitioners. This study is mainly a CFD modeling-based study conducted in ANSYS Fluent. The model parameters were validated by data generated from hydraulic tracer experiments and subsequently, simulations were performed to numerically quantify the impact of design configurations on the flow field and treatment efficiency to achieve the objectives of the paper.

2. Methodology

The overall methodology of this study has been depicted in a flow diagram (Fig. 1). First, hydraulic tracer experiments were conducted in a mesocosm scale model tank (0.3 m^3) representing a typical stormwater pond. The slope of the tank side walls was adopted from a New Zealand pond (Khan et al., 2019). An FTW made with styrofoam scaffold planted with 8 *Carex fascicularis* plants and covering 10% of water surface was placed in the tank. Then hydraulic tracer experiments were conducted for 4 cases with varying FTW geometry to produce RTD curves. Following the experiments, the experimental RTD curves were simulated in ANSYS Fluent and model parameters (meshing, turbulence model, permeability) were adjusted until a good agreement between the modeled and experimental RTD curves were reached. Once the model parameters were validated, a total of 36 cases (including the 4 validation cases) were simulated in ANSYS Fluent with varying design configurations (inlet-outlet, FTW geometry and FTW position) to determine hydraulic performance from the RTDs, flow fields and treatment efficiencies.

2.1. Hydraulic tracer experiments

The purpose of conducting hydraulic tracer experiments was to generate data for ANSYS Fluent model validation. Tracer experiments for each case were duplicated. The hydraulic tracer experiment was carried out in a tank of 0.4 m^3 (400 L) capacity filled up to 0.3 m^3 (300 L). The tank dimensions were 1.784 m (L) × 1.2 m (W) × 0.225 m (D) with a side slope of 2:1 (horizontal:vertical), representing a typical stormwater pond. The tank was constructed with a transparent polycarbonate sheet fitted in a steel frame. The inlet and outlet pipe dimensions were 0.03 m and 0.044 m, respectively. Styrofoam was used as the floating bed, which was planted with *Carex fascicularis* – a native Australian species. *C. fascicularis* has fibrous root matrix, i.e., individual root diameter <2 mm. There were four different geometries of FTW, such as rectangular, circular, triangular and L-shaped for the tracer experiments. In all of the cases, FTW covered 10% area of the water surface, which is a typical coverage of field-scale FTWs (Nuruzzaman et al., 2021; Pavlineri et al., 2017). Eight plants were planted in the floating bed, which gives the FTW a vegetation density of 40 plants/m^2. Measuring the volume of the plant roots and the FTW root zone, the porosity of the root zone was calculated to be 0.98. The submergence depth of the floating bed was 3 mm only. The length of the root zone was 0.14 m (140 mm). In all of the cases, the FTW was placed at the center of the tank. The flow rate was fixed at 0.236 L/s with a nominal hydraulic residence time (HRT) of 1271 s (21.2 min), allowing to maintain an overall laminar and sub-critical flow condition in the tank and representing the natural flow condition in a typical stormwater pond (García et al., 2020; Schmid and Hengl, 2017).

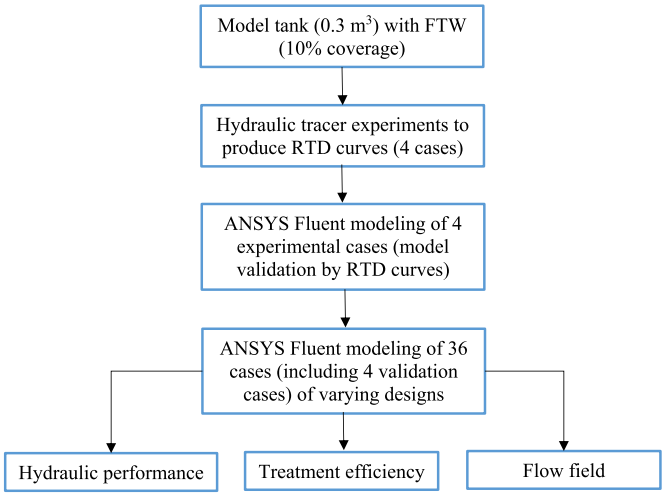

Fig. 1. Flow diagram of the overall methodology of this study.

Water in the tank was supplied from a 1000 L intermediate bulk container (IBC) by using a centrifugal pump. Before starting each experiment, the water in the IBC was mixed well for 30 min to ensure the water was homogenous in terms of electrical conductivity (EC). The roots of the plants were also washed well to prevent any increase in EC. It was also tested whether the plant roots added or decreased the EC of water due to any root secretion or uptake of any dissolved matter in the water. Plant roots were found not to change the EC of water at all in a 1-h duration and thus, the EC measurements were not influenced by the plants. Flow rate was stabilized to a constant flow rate at the outlet of the tank before injecting the tracer. Sodium chloride (NaCl) tracer was used for all experiments. To prevent density induced stratification as encountered by Bodin et al. (2012) using lithium chloride, the distance and injection time required to ensure that the tracer is fully mixed with flowing water before entering the tank was calculated using the following formula (Schmid and Hengl, 2017):

$$x = \frac{C_{tr}\,(0.802 - 0.002T_w)\,h}{0.0694\rho} * \frac{{R_h}^{4/3}}{(n\,\bar{u})^2} \tag{1}$$

$$C_{tr} = \frac{M_{tr}}{Q\Delta t} \tag{2}$$

where M_{tr} is the tracer mass (gm), Q is the flow rate (m^3/sec), Δt is the injection pulse duration (s), T_w is the water temperature (^oC), ρ is the density of water (g/m^3 for use in equation), n is the Manning's roughness coefficient of pipe wall (s/$m^{1/3}$), R_h is the hydraulic radius (m), h is the depth of flow (m) and $\bar{u}$ is the flow velocity (m/s).

A solution of 250 mL containing 10 gm of NaCl was pulse injected at 1 m upstream of the inlet (required distance was 0.3 m). By the time, NaCl enters the tank, its concentration is about 1.04% and with further dilution with the water in the tank, chances of density stratification were extremely low. Furthermore, a high percentage of mass recovery (78–86% within twice the nominal hydraulic residence time) indicated that density stratification did not occur in the experiments. The increase in EC over time at the outlet was recorded every second using a conductivity probe. Measurement continued up to twice the nominal hydraulic residence time (HRT) of the tank (21.12 min), i.e. up to 42.24 min. The EC measurements were converted to the amount of NaCl exiting with the outflow by using the following equation, which was developed by conductivity measurements of water with different amounts of NaCl (Fig. S1).

$$x = 18176 * EC \tag{3}$$

where x is the amount of NaCl in percentage (by weight) in the solution and EC is the measured increase of electrical conductivity in μS/cm.

Residence Time Distribution (RTD) curve was drawn by plotting the amount of NaCl exiting over time. The tail of the RTD was extended up to three times the nominal HRT by assuming an exponential decay function, which is a far more accurate approach than truncating the RTD at an earlier time (Fogler and Brown, 2006; Kadlec and Wallace, 2008). Normalized RTD curves were used to calculate the hydraulic performance indices. Normalization of tracer concentration and time were performed according to the following equations (Khan et al., 2013a).

$$C' = \frac{C}{C_0} \tag{4}$$

$$t_n = \frac{t}{t_{HRT}} \tag{5}$$

where C' is the normalized concentration, C is measured concentration of tracer (mg/L), C_0 is the ratio of injected tracer mass to the tank volume (mg/L), t_n is the instantaneous normalized time, t is time (min), t_{HRT} is the nominal hydraulic residence time (min).

Following the derivation of RTD curves, multiple hydraulic performance indices were calculated as follows:

$$\text{Short} - \text{circuiting index}, S_t = 1 - \frac{t_i}{t_{HRT}} \tag{6}$$

$$\text{Moment Index}, M_I = 1 - M_f \tag{7}$$

$$M_f = \int_0^1 (1 - t_c')C'\,dt' \tag{8}$$

$$\text{Hydraulic efficiency}, \lambda = \frac{t_{p1}}{t_{HRT}} \tag{9}$$

$$\text{Effective volume ratio}, e = \frac{t_{RTD}}{t_{HRT}} \tag{10}$$

$$\text{Time lapsed between } t_{90} \text{ and } t_{10}, M_{90-10} = \frac{t_{90} - t_{10}}{t_{HRT}} \tag{11}$$

$$\text{Time lapsed between } t_{75} \text{ and } t_{25}, M_{75-25} = \frac{t_{75} - t_{25}}{t_{HRT}} \tag{12}$$

$$\text{Morril index}, M_o = \frac{t_{90}}{t_{10}} \tag{13}$$

The above-mentioned indices describe short-circuiting and mixing phenomenon as well as volumetric efficiency of the pond. A detailed description of these metrics can be found in literature (Farjood et al., 2015; Khan et al., 2013a; Nuruzzaman et al., 2021; Wahl et al., 2010).

2.2. Numerical simulation in ANSYS fluent

2.2.1. Modeling description

The numerical simulation was conducted in ANSYS 2021 R2 Fluent Solver (ANSYS Inc, 2015). Reynolds averaged Navier-Stokes (RANS) modeling approach was adopted for the 3D transient simulation. For a steady and incompressible flow, the conservation of mass and momentum equations of the RANS model are:

$$\rho\frac{\partial u_i}{\partial x_i} = 0 \tag{14}$$

$$\rho\frac{\partial u_i u_j}{\partial x_j} = -\frac{\partial p}{\partial x_i} + \mu\frac{\partial^2 u_i}{\partial x_j \partial x_j} - \rho\frac{\overline{\partial u_j' u_i'}}{\partial x_j} + f_i \tag{15}$$

where ρ is the density of water, u_i is the instantaneous velocity, i and j represent the directions along the stream (x), cross-stream (y) and vertical directions (z), respectively; $\overline{u_j' u_i'}$ denotes the Reynolds stress; u' represents the fluctuating potion of the velocity; p denotes the pressure; μ is the dynamic viscosity of water; f_i represents the drag of the root zone, which is a momentum sink.

The transition shear stress transport (SST) model was used as the turbulence model. This model was able to describe the experimental RTDs of our study better than any other available turbulence model in ANSYS Fluent. It was also used by Xavier et al. (2018) and Yamasaki et al. (2022) where good model validations were obtained. The transition SST model couples the SST k-ω model with intermittency and transition momentum-thickness Reynolds number.

The turbulent kinetic energy, k and the specific dissipation rate, ω of the SST model are described in the following forms (ANSYS Inc, 2015):

$$\frac{\partial}{\partial t}(\rho k) + \frac{\partial}{\partial x_i}(\rho k u_i) = \frac{\partial}{\partial x_j}\left(\Gamma_k\frac{\partial k}{\partial x_j}\right) + G_k - Y_k + S_k \tag{16}$$

$$\frac{\partial}{\partial t}(\rho\omega) + \frac{\partial}{\partial x_i}(\rho\omega u_i) = \frac{\partial}{\partial x_j}\left(\Gamma_\omega\frac{\partial \omega}{\partial x_j}\right) + G_\omega - Y_\omega + D_\omega + S_\omega \tag{17}$$

where G_k is the turbulent kinetic energy generation due to velocity gradients, G_ω is the generation of specific dissipation rate, Γ_k and Γ_ω are effective diffusivities of k and ω. Y_k and Y_ω are the dissipation of k and ω

due to turbulence. D_ω is the cross-diffusion.

The transport equations of the transition model for intermittency (γ) and transition momentum thickness Reynolds number ($Re_{\theta t}$)are as follows:

$$\frac{\partial}{\partial t}(\rho\gamma)+\frac{\partial}{\partial x_j}(\rho u_j\gamma)=\frac{\partial}{\partial x_j}\left[\left(\mu+\frac{\mu_t}{\sigma_\gamma}\right)\frac{\partial}{\partial x_j}\right]+P_{\gamma 1}-E_{\gamma 1}+P_{\gamma 2}-E_{\gamma 2} \tag{18}$$

$$\frac{\partial}{\partial t}(\rho Re_{\theta t})+\frac{\partial}{\partial x_j}(\rho u_j Re_{\theta t})=P_{\theta t}+\frac{\partial}{\partial x_j}\left[\sigma_{\theta t}(\mu+\mu_t)\frac{\partial Re_{\theta t}}{\partial x_j}\right] \tag{19}$$

where P_γ and E_γ are transitions sources, μ_t is the turbulent viscosity.

The coupling of SST transport equations and the transition model is described as:

$$\frac{\partial}{\partial t}(\rho k)+\frac{\partial}{\partial x_j}(\rho u_j k)=P_k-D_k+\frac{\partial}{\partial x_j}\left[(\mu+\sigma_k\mu_t)\frac{\partial k}{\partial x_j}\right] \tag{20}$$

where P_k is the shear production rate, σ_k is the turbulent Prandtl number for k,

Default values for all model constants were used. Further details of the Transition SST modeling parameters and constants can be found in (ANSYS Inc, 2015; Menter et al., 2003; Xavier et al., 2018).

2.2.2. Model validation

We adopted the approach of Xavier et al. (2018) to validate our ANSYS Fluent model, i.e. matching experimental RTDs with simulated RTDs. First, the geometry of the experimental tank was created with the root zone represented as a porous zone in ANSYS Fluent. The drag due to the porous media is expressed as follows:

$$f_i=-\left(\underbrace{\frac{\mu}{K_{perm}}u_i}_{viscous\ drag}+\underbrace{\frac{1}{2}C_2\rho|u_i|u_i}_{inertial\ drag}\right) \tag{21}$$

where K_{perm} is the permeability of the porous media and C_2 is the inertial drag coefficient.

Initially, Ergun equation was used to estimate the values of both K_{perm} and C_2 for root diameters between 0.1 mm and 2 mm. The results from Ergun equation did not produce a good agreement between experimental and modeled RTDs for any root diameter. Sonnenwald et al. (2016a) used Ergun equation, which also failed to validate their model. The CFD model is highly sensitive to the inertial drag (Sonnenwald et al., 2016a). As such, a little variation in the value of the inertial drag coefficient (C_2) produces a large change and it makes it harder to validate the model. A small error in estimating the diameter of the roots or porosity of the root zone influence the model significantly due to the high sensitivity of C_2. The root diameter is not uniform and not bundled together uniformly, which renders the use of Ergun equation impractical and incorporating inertial drag resistance into the model less accurate. Furthermore, from the experimental results of Kundu et al. (2016), it was found that inertia dominated flow regime (Forchheimer inertial regime) started at a velocity of 0.05 m/s within the porous media. This means that at a lower velocity (<0.03 m/s), inertial resistance does not play any role to the drag exerted by a porous media. The mean flow velocity within the tank of our study was 0.0014 m/s. The mean velocity within the porous media is estimated to be well below 0.03 m/s despite the presence of small portions of localised high velocity areas. Therefore, based on the estimated velocity ranges, it can be argued that exclusion of inertial resistance will not have any significant effect on the flow field.

Xavier et al. (2018) ignored the inertial drag and achieved a good model validation. We also ignored the inertial drag to achieve better agreement between experimental data and model outputs. Trial and error approach was used to find the value of K_{perm} to be 2×10^{-6} m^2 to best match the experimental RTD curves. Xavier et al. (2018) used the data of Khan et al. (2013a) and found the value of K_{perm} to be 10^{-7} m^2, which produced best matching between modeled and experimental data. The value of K_{perm} of the FTW root zone in the Yamasaki et al. (2022) study was found to be 1.418×10^{-5} m^2. From the range of K_{perm} found in literature, the value of K_{perm} found in this study seems reasonable. Yamasaki et al. (2022) used the Ergun equation to estimate the K_{perm} and C_2 values in their study. Estimates of K_{perm} and C_2 based on Ergun equation was able produce a good match between experimental and modeled velocity profiles in their study because Yamasaki et al. (2022) validated their model from the experiments of Liu et al. (2019) where the roots were made of rigid dowels with uniform diameter.

Tetrahedral and hexahedral meshing methods were adopted for the fluid domain and porous zone, respectively, with finer mesh sizes near the porous zone, inlet, outlet and boundary walls (Fig. S2). The water surface was defined as a symmetry (Xavier et al., 2018). A total of 1.5 million tetrahedral and hexahedral cells were created for the CFD simulation. Mesh independent test revealed that any further finer size mesh would not achieve significantly better results but would rather increase the computational burden. For comparison, Xavier et al. (2018) used 100,000 hexahedral cells for a 700 L tank and Khan et al. (2013b) used 72,000 nodes (equivalent to 200,000 tetrahedral cells) for their model.

In the transient simulation, once the flow rate in the outlet was stabilized (typically within 200–300 s), the tracer was injected over a 3-s period as a discrete phase mass with a total of 52,224 particles. It is noteworthy that the hydraulic tracer experiment was conducted using soluble tracer (NaCl) and diffusion effect has a potential role in the mixing process of soluble tracer whereas insoluble particle tracing was used in ANSYS Fluent to simulate the tracer experiment. The concentration of the NaCl solution was about 1.04% at the time it entered into the tank, which is a very low concentration. According to Fick's law, the diffusion of a solute is directly proportional to its concentration gradient (Faupel, 1992; Paul et al., 2014). At a very low concentration, the concentration gradient is also very low and therefore, the diffusion effect played a negligible role in the experiments. Furthermore, as the tracer moved forward in the tank, its concentration was reduced further down, preventing any further diffusion. The concentration of the solution was primarily chosen to prevent density stratification and at the same time it served the purpose of minimizing diffusion of tracer. Therefore, the simulation of hydraulic tracer experiments in ANSYS Fluent using particle injection was deemed appropriate. Tracer mass exiting at the outlet was sampled over time. The simulation and tracer mass monitoring at the outlet was performed until 63.5 min (3 times t_{HRT}) after the tracer injection, from which the simulated RTD curves and hydraulic performance indices were calculated. Once the experimental RTDs and simulated RTDs were in good agreement, a total of 36 cases were simulated by varying the inlet–outlet, FTW position and FTW geometry configurations as depicted and labeled in Fig. 2.

2.2.3. Pollutant mass removal calculation

ANSYS Fluent allows for tracking discrete phase particles with individual particle IDs. The fraction of particles coming in contact with the FTW within the FTW was calculated by sampling the discrete particles within the porous zone. This information facilitated the estimation of mass removal for a steady state condition. Mass removal was estimated by using the first-order kinetic equation as follows:

$$R\ (\%)=f\left(1-e^{-k_r\left(\frac{V_r}{Q_r}\right)}\right)\times100 \tag{22}$$

where f is the fraction of tracer mass coming in contact with the floating wetland, k_r is the removal rate within FTW, V_r is the volume of root zone (m^3), Q_r is the flow rate to the root zone (m^3/sec).

In equation 22, the term V_r/Q_r equals to the residence time within FTW (t_r). The non-dimensional removal rate $k_r\left(\frac{V_r}{Q_r}\right)$ in equation 22 is equivalent to the FTW system scale non-dimensional removal rate kt_{HRT}

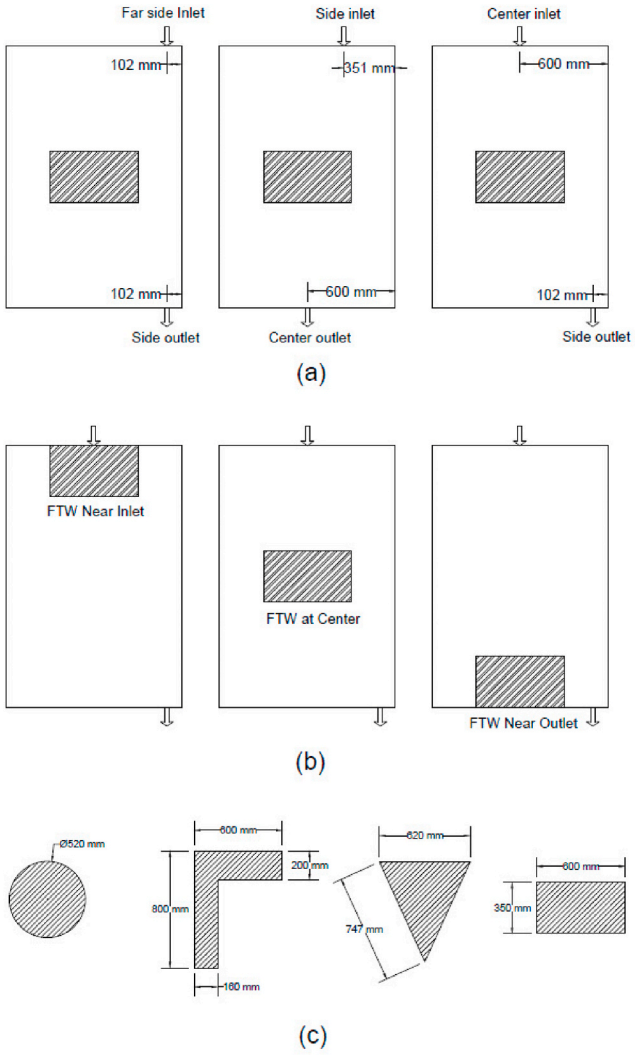

Case ID	FTW Shape	FTW Position	Inlet-Outlet
C-1	Circular	Near inlet	Far Side-Side
C-2	Circular	Center	Far Side-Side
C-3	Circular	Near outlet	Far Side-Side
C-4	Circular	Near inlet	Side-Center
C-5	Circular	Center	Side-Center
C-6	Circular	Near outlet	Side-Center
C-7	Circular	Near inlet	Center-Side
C-8	Circular	Center	Center-Side
C-9	Circular	Near outlet	Center-Side
L-1	L	Near inlet	Far Side-Side
L-2	L	Center	Far Side-Side
L-3	L	Near outlet	Far Side-Side
L-4	L	Near inlet	Side-Center
L-5	L	Center	Side-Center
L-6	L	Near outlet	Side-Center
L-7	L	Near inlet	Center-Side
L-8	L	Center	Center-Side
L-9	L	Near outlet	Center-Side
R-1	Rectangular	Near inlet	Far Side-Side
R-2	Rectangular	Center	Far Side-Side
R-3	Rectangular	Near outlet	Far Side-Side
R-4	Rectangular	Near inlet	Side-Center
R-5	Rectangular	Center	Side-Center
R-6	Rectangular	Near outlet	Side-Center
R-7	Rectangular	Near inlet	Center-Side
R-8	Rectangular	Center	Center-Side
R-9	Rectangular	Near outlet	Center-Side
T-1	Triangular	Near inlet	Far Side-Side
T-2	Triangular	Center	Far Side-Side
T-3	Triangular	Near outlet	Far Side-Side
T-4	Triangular	Near inlet	Side-Center
T-5	Triangular	Center	Side-Center
T-6	Triangular	Near outlet	Side-Center
T-7	Triangular	Near inlet	Center-Side
T-8	Triangular	Center	Center-Side
T-9	Triangular	Near outlet	Center-Side

Fig. 2. Design configurations of the simulated cases. (a) inlet and outlet variation (b) FTW position variation (c) FTW geometry variation. A total of 36 cases were considered covering all possible combinations of the three design configurations.

where k is the system scale removal rate (per day) and t_{HRT} is the nominal HRT of the tank. The system-scale FTW represents the whole tank including the FTW. It was assumed that pollutant removal occurred only within the root zone and not any other areas of the tank. As such, the system scale removal rate (k) was converted to removal rate within FTW only by equation (23) (Xavier et al., 2018).

$$k_r = k\left(\frac{V}{V_r}\right) \tag{23}$$

where V is the volume of the tank (m^3).

To attain equal mass removal for a particular design configuration at different physical scale, the non-dimensional removal rate $k_r\left(\frac{V_r}{Q_r}\right)$ needs to be the same. The removal rate $k_r\left(\frac{V_r}{Q_r}\right)$ will be the same at different physical scale, if the product of k_r and t_{HRT} are same without changing the design configurations of the system. It implies that $V_r/\ Q_r$ will change proportionally with the change of t_{HRT} to satisfy the equal mass removal condition. Xavier et al. (2018) confirmed that to attain similar mass removal of geometrically similar systems, but at a different physical scale and different nominal HRT (t_{HRT}), the non-dimensional parameter $k_r t_{HRT}$ needs to be the same. This allowed us to conduct simulations at a smaller scale and scale up the results to understand pollutant mass removal at a larger physical scale (field-scale) and for different nominal HRT as also applied by Liu et al. (2019) and Yamasaki et al. (2022) using the same principle. Xavier et al. (2018) estimated that the value of days $k_r t_{HRT}$ could vary between 0.43 and 20 based on the reported first-order kinetic rates within FTW (between 0.43 and 1.28 per day) and typical nominal HRT in field-scale ponds (between 1 and 16 days). Pollutant mass removal was calculated by varying the value of k_r within 0.000393 s^{-1} and 0.015736 s^{-1} to achieve $k_r t_{HRT}$ within 0.5 and 20. Yamasaki et al. (2022) used the value of k_r from 0.0012 to 0.12 s^{-1} to achieve the same $k_r t_{HRT}$ for their study.

2.3. Statistical analysis

Statistical tests were conducted to indicate the significance of different variables within a design configuration on pollutant mass removal. The percent removal data were variable-wise clustered and appropriate tests were conducted for different $k_r t_{HRT}$. Kruskal-Wallis non-parametric test (equivalent to one-way ANOVA) was conducted where normality and homogeneity of variance assumptions were both violated (McKight and Najab, 2010). One-way ANOVA with Games-Howell post-hoc analysis was performed where only homogeneity of variance was not found (Hilton and Armstrong, 2006). Sensitivity analysis was performed to figure out the most important design configuration out of the three. The analysis was performed by clustering the percent removal data keeping two configurations constant and

varying the third. For example, when the sensitivity of FTW geometry was estimated, the data for all far side inlet–side outlet and FTW near inlet position cases were clustered where the FTW geometry was variable. Then for each of the clusters, the sensitivity index was calculated as (Hamby, 1994; Hoffman and Gardner, 1983):

$$S_I = \frac{D_{max} - D_{min}}{D_{max}} \quad (24)$$

where D_{max} is the maximum value of the cluster, D_{min} is the minimum value of the cluster.

This process was continued for all combinations. Once the S_I for all clusters was derived, the median values of S_I were calculated for each design configuration at different $k_r t_{HRT}$.

3. Results and discussion

3.1. Tracer experiments and model validation

Tracer experiments were conducted as outlined in section 2.1 to generate RTD curves for model validation. The normalized experimental and simulated RTD curves for four selected cases (C-8, L-8, R-8 and T-8) are presented in Fig. 3 for comparison. The model was able to predict the experimental RTDs with fair accuracy. R^2 values for the experimental vs. simulated RTDs were found to range between 0.70 and 0.81. Root Mean Square Error (RMSE) was calculated to range between 0.05 and 0.11. Apart from the error indicators, the simulated RTDs were closely following the experimental RTDs from visual observation. When calculating different hydraulic performance indices from experimental and simulated RTDs, the indices were nearly identical and the difference was less than 10%. For example, experimental normalized t_{mean} for circular, L-shaped, rectangular and triangular FTWs were 0.79, 0.71, 0.80 and

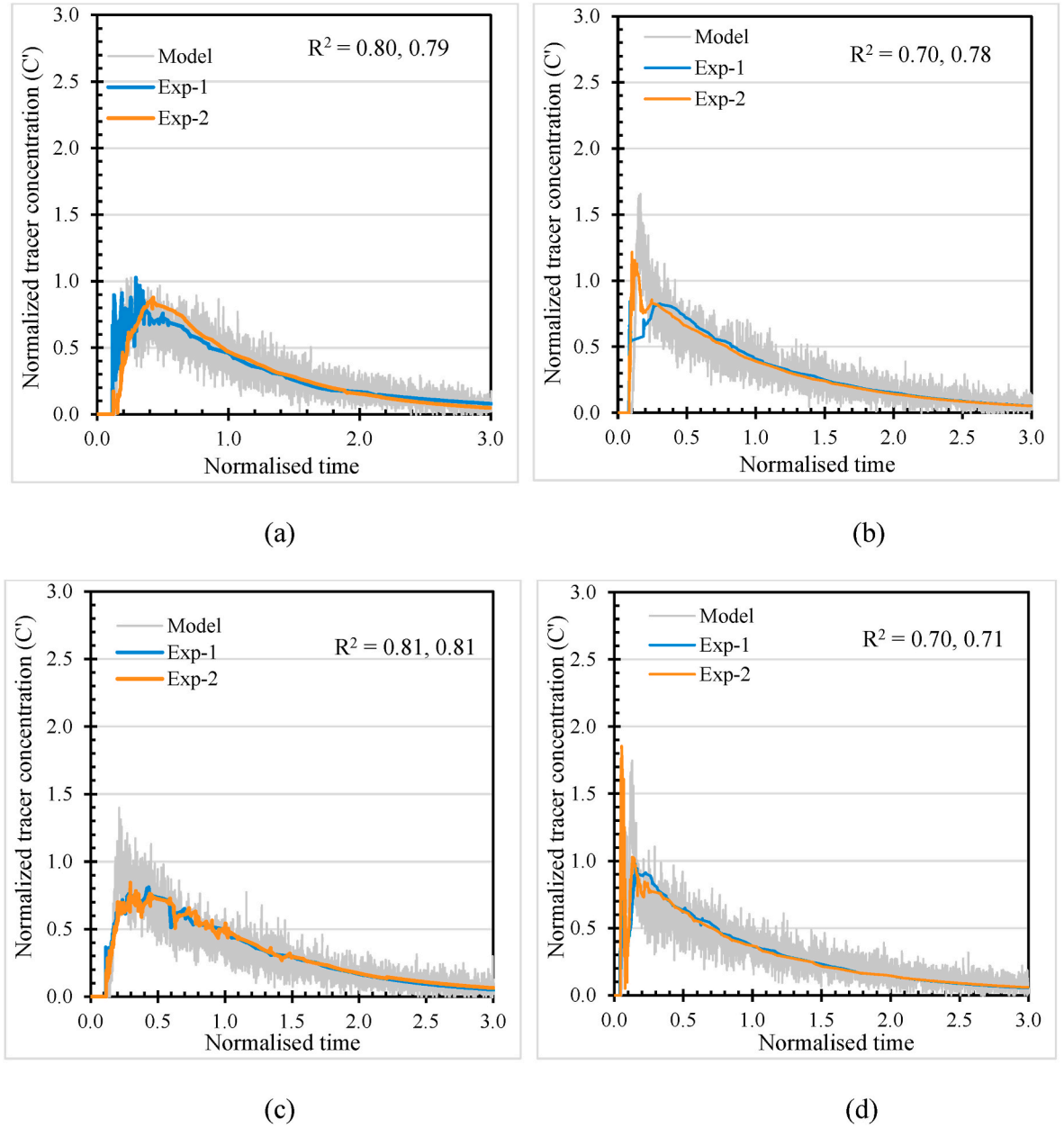

Fig. 3. Comparison between experimental and ANSYS Fluent simulated RTD curves for different geometries of FTW (a) Case C-8 (b) Case L-8 (c) Case R-8 (d) Case T-8. Two tracer experiments were conducted for each case to reproduce the experiments.

0.69, respectively (Table S1), whereas the simulated values were 0.86, 0.75, 0.81 and 0.76, respectively.

RTD curves can reflect multiple processes and phenomena related to flow field of a pond, e.g., dispersion, advection, short-circuiting and presence of dead zones. Therefore, CFD model validation by RTD curves is a robust method and can reflect the flow filed accurately. Nevertheless, verification of velocity profiles could further strengthen the model validation. Measurement of velocity profiles of our experiments could not be carried out due to lack of measurement instruments suitable for low velocities. However, to deduce how realistic the velocity profiles of this study are, the velocity profiles of the root zone and under the root zone of this study were compared with a typical velocity profile for suspended canopies (in this case plant roots). The main feature of flow profile of a suspended canopy is that the velocity is significantly lower within the canopies compared to the velocity under the canopies where water can flow freely (Plew, 2011) as also found in this study (Fig. S3). Velocity decelerates within the canopies due to resistance. Velocity is high under the canopies due to absence of any resistance exerted by the canopies. These features were dominant in all cases. Flow velocity in case L-8 was relatively higher than the other three validation cases. The L-shaped FTW intercepted the high-velocity stream at a point where the stream wise length of the FTW was lower than the other three cases and hence, flow deceleration was not as profound as the other three validation cases. These are realistic representations of the velocity profiles in the CFD model. Therefore, producing good agreement between modeled and experimented RTDs as well as having realistic flow velocity profiles found in this study, it can be strongly argued that the flow fields modeled in this study are accurate and further simulation results conducted in this study can be considered accurate.

3.2. Simulation results of tracer experiments in ANSYS fluent

Following a satisfactory model validation, simulations were performed for all 36 cases of this study. Normalized RTD curves were plotted for visual observation (Fig. S4) and subsequently, hydraulic performance indices were calculated (Table S1). Tracer mass recovery ranged between 81 and 96%, which indicates a satisfactory hydraulic tracer study (Bodin et al., 2012; Kadlec and Wallace, 2008). The RTDs demonstrate that for far side inlet–side outlet cases, the peak of the RTD reached very quickly and was always profoundly sharp, indicating high short-circuiting. Low normalized t_{mean} (<0.04) and high $S_{c(16)}$ (>0.98) confirms that far side inlet–side outlet cases coupled with FTWs positioned at the center promoted short-circuiting to an extreme level. It is to be noted that when t_{mean} is normalized by nominal HRT, it equals the volumetric efficiency (e). As such, volumetric efficiency is also low for far side inlet–side outlet cases. Center inlet–side outlet configurations for FTWs placed near inlet and at the center were characterized by higher hydraulic efficiency. It implies a delay in the peak of RTDs and better hydraulic performance. The initial arrival time of tracer (S_i) was also delayed for these cases, indicating a longer and slower flow path. This condition was created by the presence of FTW on the flow path between the inlet and outlet, which acts as a resistance to the flow. Volumetric efficiency for all cases except for the side inlet–side outlet cases was mostly greater than 0.75, suggesting the presence of an only small amount of dead zone within the tank (Persson and Wittgren, 2003). It signifies the importance of proper placement of inlet and outlet in a stormwater pond.

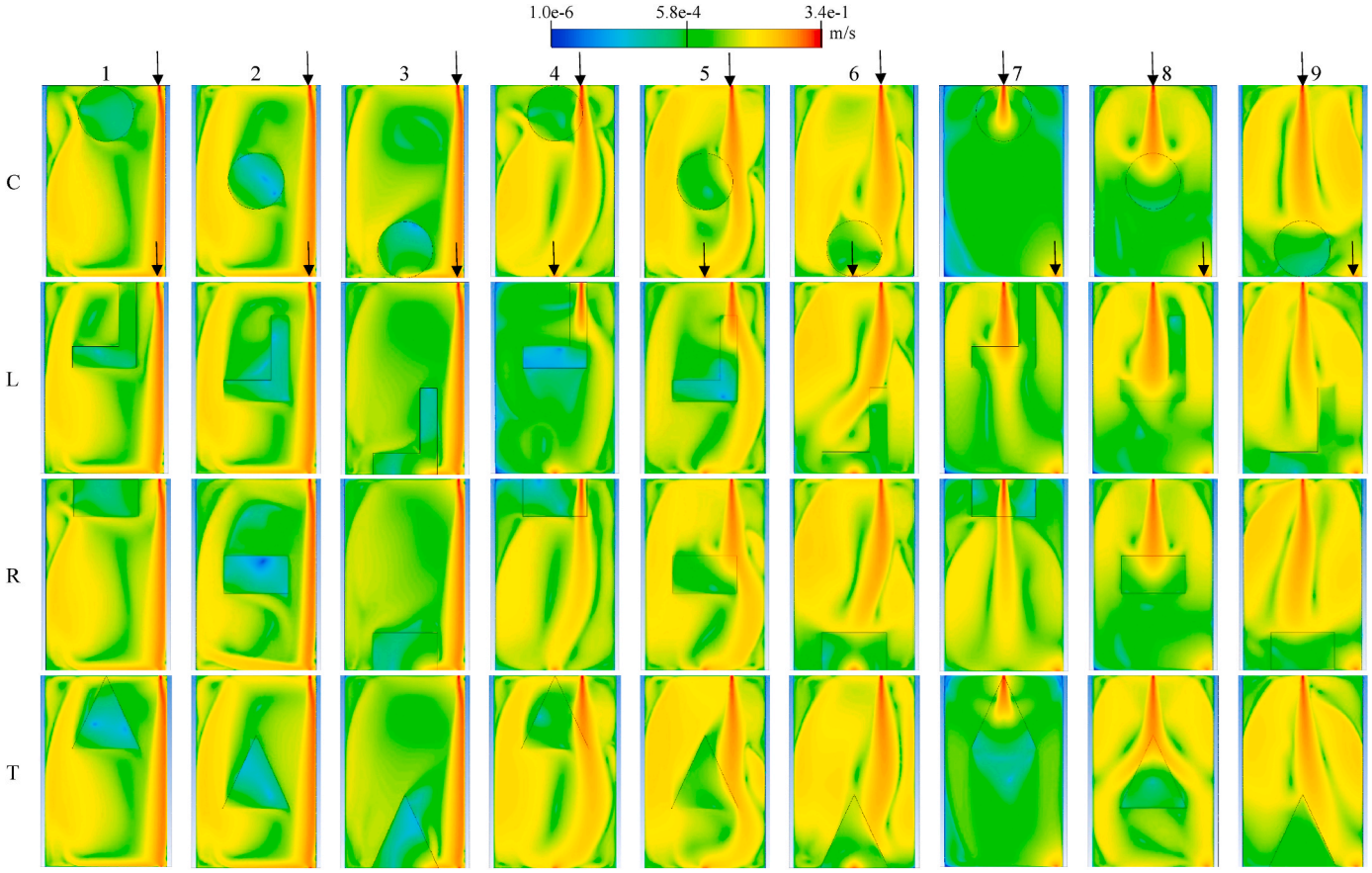

Fig. 4. Velocity contours of all simulated cases. The contours are on a horizontal plane passing through the middle of the inlet at a water depth of 0.204 m. Arrows in the first row indicate the location of inlet and outlet. The red color represents the high-velocity streams. Different discernible shapes are the FTWs. (For interpretation of the references to color in this figure legend, the reader is referred to the Web version of this article.)

3.3. Flow field

Velocity contours were generated on a horizontal plane passing through the midpoint of the inlet cross-section (water depth = 0.204 m) to visually observe the flow field (Fig. 4). The red color represents the highest velocity magnitude, followed by orange, yellow, green, cyan and blue. Small recirculation zones were created on the corners and flow within the porous zone is marked by low velocity, which is a realistic representation of the actual flow field (Khan et al., 2013b; Sonnenwald et al., 2016b; Xavier et al., 2018). The continuous presence of high-velocity stream from the inlet until outlet for far side inlet–side outlet cases visually demonstrates how little the inflow is interacting with the FTW and how profound the short-circuiting phenomenon is in these cases. The high-velocity stream is diffused and often cut off for other inlet–outlet cases and especially when the FTW is placed near the inlet. The position of the FTW guides the high-velocity stream and its diffusion length with FTW placed near the outlet had the most extended jet length. FTW placed near inlet also appears to have more flow uniformity in the tank compared to other positions. The visual observation of the velocity fields corroborates the hydraulic performance of the cases. For example, far side inlet–side outlet cases performed poorest in terms of hydraulic performance with the highest level of short-circuiting. Conversely, FTW placed near the inlet mostly performed better than other positions achieving plug flow condition ($M_I >$ 0.6). In a plug flow condition, the residence time of the flowing water is uniform and close to the nominal HRT. Xavier et al. (2018) found that FTW placed near inlet receiving high-velocity stream and diffusing it achieved higher pollutant mass removal compared to other positions. This phenomenon will be examined in the next section through treatment efficiency. The flow field seemed to have been less affected by the

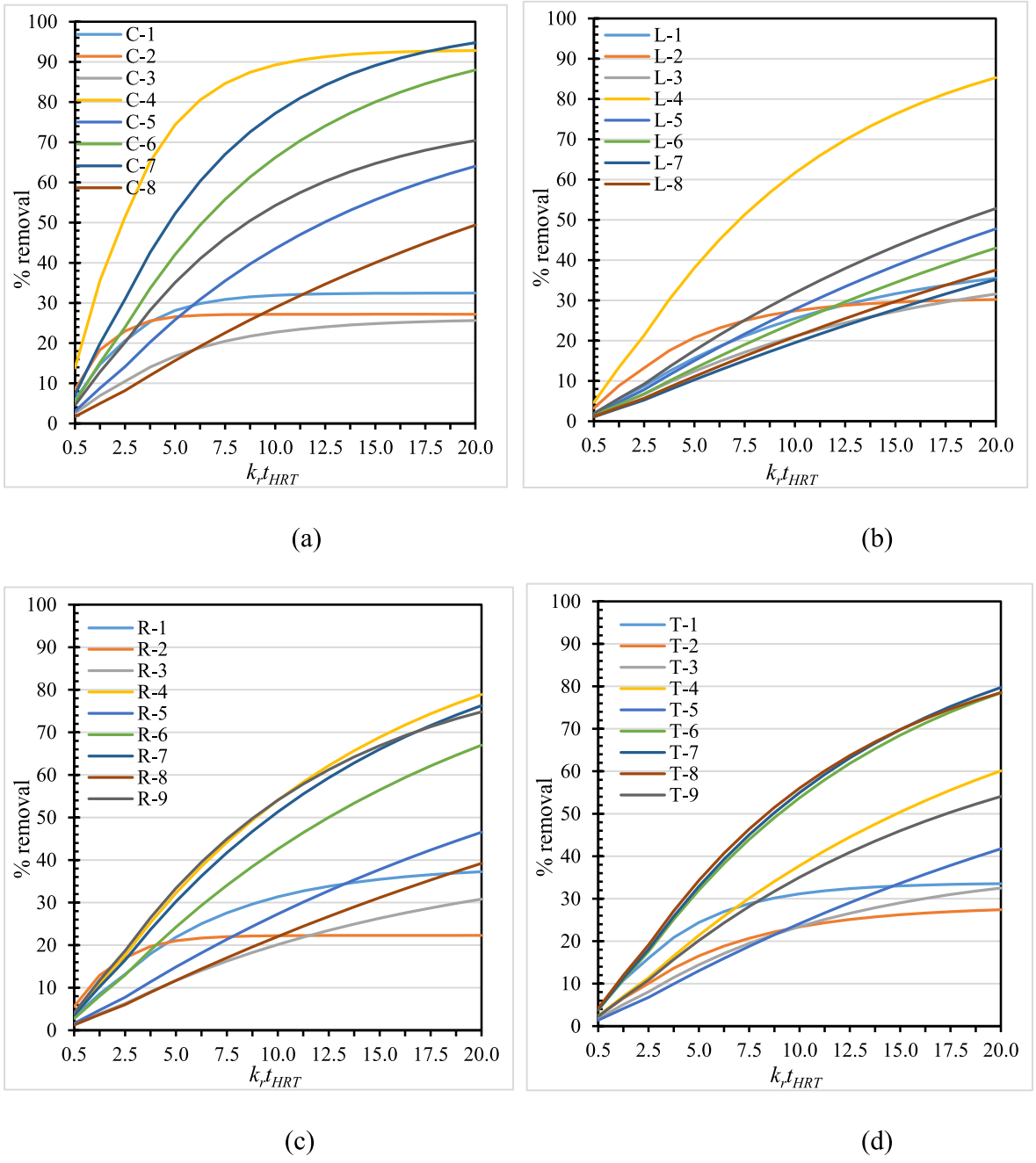

Fig. 5. Treatment efficiency of different design configurations for variable krtHRT values. (a) Cases C1–C9 (b) Cases L1–L9 (c) Cases R1–R9 (d) Cases T1–T9.

geometry of FTW compared to the other two design configurations.

3.4. Pollutant mass removal

Percent pollutant removal was estimated using equation 22 for all cases for variable values of $k_r t_{HRT}$. It is notable that at $k_r t_{HRT}$ >10, there was little to no increase of pollutant mass removal for the far side inlet–side outlet cases regardless of FTW geometry and position (Fig. 5). Mass removal of these cases was mainly limited by mass supply, i.e., the fraction of mass entering into FTW (Table S2). Geometry-wise, circular FTWs were removing a higher amount of mass (up to 94.8%) compared to other geometries.

To be able to better interpret the effect of the variables of the design configurations, the data was split according to design configurations and the mean was compared between variables of each design configuration as presented in Table 1. One of the key observations from statistical analysis is that at low values of the non-dimensional removal parameter $k_r t_{HRT}$, there is no significant impact of inlet–outlet configuration (for $k_r t_{HRT}$ <10) and position (for $k_r t_{HRT}$ <5) on the percent removal. As the non-dimensional removal rate increases, the impact of the variables of these two design configurations becomes profound. This happened due to the fact that the removal was mainly governed by the residence time within the FTW for these cases. As the value of $k_r t_{HRT}$ increases, percent removal will increase unless it is limited by the fraction of flow coming in contact with the FTW. It implies that at high $k_r t_{HRT}$, given that there is enough supply of pollutant mass to the FTW, it is possible to achieve an overall high removal. It was observed that for far side inlet–side outlet cases, between 27 and 43% of the inflow was entering the FTW, which resulted in significantly lower pollutant removal for this particular inlet–outlet configuration. It means that at high $k_r t_{HRT}$, even though the removal was happening very fast, there was not enough supply of pollutant mass to the FTW to achieve an overall high removal. Conversely, for the other two inlet–outlet configurations, mass entry to the FTW ranged from 77% to 100% and at a higher removal rate, pollutant mass removal was also high. When the FTW was positioned at the center, a lower fraction of inflow was entering the FTW compared to other positions, especially when coupled with the far side inlet–side outlet, which led to a low percentage of mass removal. On the other hand, when comparing different geometries of FTWs, it is noteworthy that the difference in percent removal between different geometries was only significant at low $k_r t_{HRT}$ (<10). At high $k_r t_{HRT}$ (≥10), no significance was observed between geometries, which was predominantly due to variance in residence time for variable FTW geometries. The fraction of inflow entering FTW averaged between 70.8 and 78.5% for different geometry, which is not a large difference. However, for a nominal HRT of 1271 s, the residence time within FTW averaged 306, 90, 165 and 130 s for circular, L-shaped, rectangular and triangular geometries, which is more than threefold variation between the lowest and highest values. As such, at high $k_r t_{HRT}$, when the pollutant mass supply is not limited, the pollutant mass removal gap in percentage among different geometries was closing in, averting statistical significance.

It is important to note that even though there was a general trend for circular FTW geometry, side inlet–center outlet and FTW positions near inlet to perform better than other geometries, inlet–outlet configurations and positions, a combination of these design configurations may achieve higher or lower removal. For example, L-shaped geometry being the worst of all geometries on average, achieved 85.3% removal when positioned near inlet for side inlet–center outlet configurations (Case L-4). Keeping other configurations and $k_r t_{HRT}$ the same, rectangular and triangular geometries achieved 78.9% (Case R-4) and 60.1% (Case T-4) removal, respectively. The highest removal at $k_r t_{HRT} = 20$ was achieved in case C-7 (94.8%), which is a center inlet–side outlet configuration.

Values sharing common letters in superscripts are not statistically significant. The comparison was performed between variables of individual design configuration.

Statistical comparisons provided information on the differences between variables of each design configuration, but, it did not describe the relative importance of design configurations in consideration. To estimate which design configuration has most impact on pollutant mass removal, the results of sensitivity analysis are illustrated in Fig. 6. At a low removal rate ($k_r t_{HRT}$ <10), pollutant mass removal is almost equally sensitive to all design configurations. Sensitivity of all design configurations decreases as the non-dimensional removal rate increases. Sensitivity index decreased for inlet–outlet configuration initially and increased for $k_r t_{HRT}$ >10 to nearly its initial level of sensitivity (0.6). It implies that for an FTW system operating at $k_r t_{HRT}$ >10, inlet–outlet configuration plays a major role in determining the pollutant mass removal than the other two design configurations. As such, designers must be more vigilant in choosing proper inlet–outlet configurations for ponds with a higher detention period.

3.5. Relation between hydraulic performance and pollutant mass removal

An attempt was made to determine the relationship between hydraulic performance indices and pollutant mass removal by performing linear regression analysis between individual indices and pollutant mass removal at different removal rates. No significant relationship between hydraulic performance indices and pollutant mass removal was found except for M_I. A statistically significant ($p < 0.05$) positive linear relationship was found between M_I and pollutant mass removal, especially

Table 1
Statistical comparison of treatment efficiency between variables at different $k_r t_{HRT}$. The data was split according to design configurations and then variables within each design configuration were statistically compared.

Data splitting	Variable	Mean percent removal for variable $k_r t_{HRT}$				
		0.5	5	10	15	20
Geometry Wise	Circular	5.8^{a}	35.2^{a}	49.0^{a}	56.2^{a}	60.5^{a}
	L-shaped	2.1^{b}	17.1^{b}	28.9^{a}	37.6^{a}	44.3^{a}
	Rectangular	3.0^{ab}	22.4^{ab}	36.1^{a}	45.7^{a}	52.6^{a}
	Triangular	2.9^{ab}	23.2^{ab}	37.7^{a}	47.4^{a}	54.0^{a}
Inlet–Outlet wise	Side-Side	3.5^{a}	19.2^{a}	25.6^{b}	28.8^{b}	30.5^{b}
	Side-Center	3.8^{a}	28.9^{a}	46.0^{a}	57.7^{a}	66.1^{a}
	Center-Side	3.1^{a}	25.4^{a}	42.2^{a}	53.7^{a}	61.9^{a}
Position wise	Near inlet	4.6^{a}	31.8^{a}	47.1^{a}	56.1^{a}	61.8^{a}
	Center	3.0^{a}	18.9^{b}	29.2^{b}	36.8^{b}	42.7^{b}
	Near outlet	2.8^{a}	22.7^{ab}	37.5^{ab}	47.3^{ab}	54.1^{ab}

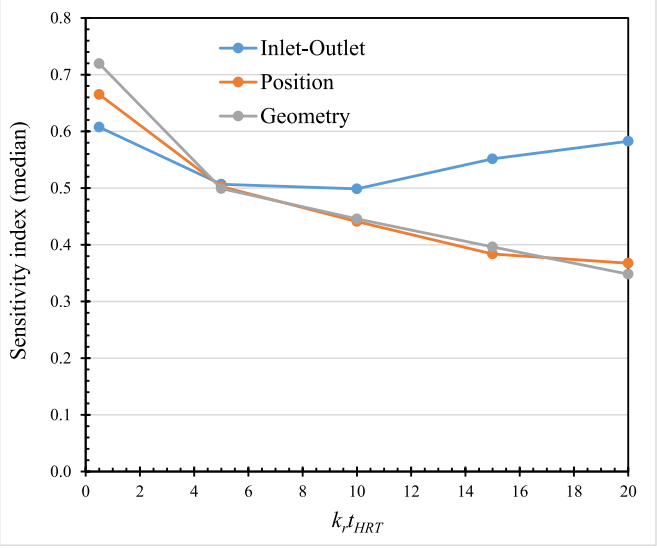

Fig. 6. Sensitivity of treatment efficiency to design configurations. The sensitivity index here represents the degree treatment efficiency will vary if the design configurations are altered.

at high removal rate. It implies that retrofitting an FTW in a stormwater pond in a way that enhances plug flow condition is preferable. The regression analysis results are presented in Table S3. Significant relationship was also detected at $k_r t_{HRT} = 10$, but with a lower R^2 value (0.24) and β (<0.5), the relationship cannot be confidently detected. At lower removal rate ($k_r t_{HRT} \leq 5$), no significance was detected ($p > 0.05$). The insignificant relationship at lower removal rate is because of lower pollutant mass removal. Since at a removal rate, the FTW is not able to remove a substantial amount of pollutant, RTD becomes irrelevant in determining mass removal. It is also interesting to find that most of the hydraulic performance indices, especially short-circuiting index failed to demonstrate a relationship with the pollutant mass removal. Short-circuiting index can indicate the fraction of pollutant mass entry to the FTW and yet it did not have any relationship with the pollutant mass removal. Therefore, regression analysis was performed for individual indices and fraction of pollutant mass entry (f), which revealed that significant relationship exist between most of the hydraulic performance indices (except λ and S_i) and f. However, treatment efficiency is also highly dependent on the residence time within FTW (t_r). It was revealed that most of the indices were not able to describe the residence time within FTW. Therefore, no relationship between the hydraulic performance indices and pollutant mass removal could be derived except for M_1. It is also important to note that pollutant mass removal in this study mainly corresponds to dissolved pollutants. As such, other hydraulic performance indices may still be able to demonstrate relationship with particulate pollutant removal, which requires further investigation.

Understanding the hydraulics of stormwater pond retrofitted with FTW is crucial for an effective treatment. Hydraulics of the pond can be manipulated by design configurations of FTW and the pond to enhance treatment efficiency. The results of our study has several design implications, which practitioners can implement in field-scale FTWs. The most profound implication is that if the positions of inlet and outlet are in such a way that a direct high velocity stream from inlet to outlet is created bypassing the FTW, it will lead to poor treatment efficiency. As such, either inlet and outlet or FTWs must be positioned in a way so that the high velocity stream can be intercepted by the FTW. Secondly, it was found that FTWs placed near the inlet has benefits in terms of enhancing treatment efficiency, which was also reported by Xavier et al. (2018). Furthermore, circular FTW geometry is superior to other geometries in terms of treatment efficiency. Circular geometry promotes the contact period between flowing water and the FTW and thus achieves higher treatment efficiency. As such, circular geometry can be adopted in field-scale FTWs.

It is important to note that dissolved pollutants are mainly removed by plant uptake and microbial activities occurring in the root zone of an FTW. Since, our assumption in this study was that the removal was occurring only in the FTW root zone, the treatment efficiency results of this study corresponds to dissolved pollutants only and not particulate pollutants. Removal of particulate pollutants work in a different mechanism, mainly by settlement. Settlement of particulate pollutant may be impacted by the altered hydraulic performance due to change in design configuration. However, this effect was not included in our study. Furthermore, removal of pollutants outside the root zone can happen due to microbial presence in the inflowing water, which is also referred as applied water body kinetics (Wang and Sample, 2013). The effect of applied water body kinetics is outside the scope of our study and the treatment efficiency results only refer to the direct contribution by the FTW.

4. Conclusions

This study investigated the impact of three design configurations (e.g., inlet–outlet, FTW position and FTW geometry) on the hydraulics and pollutant removal efficiency of FTW retrofitted in stormwater pond. It was demonstrated how these configurations influence pond flow field, hydraulic performance and pollutant mass removal efficiency. The pollutant mass removal was estimated for non-dimensional removal rate $k_r t_{HRT}$ ranging between 0.5 and 20. The following key conclusions are drawn from this study:

- Pollutant mass removal was most sensitive to inlet–outlet configurations. As such, out of the three design configurations, inlet–outlet configuration has the most profound impact on pollutant mass removal by FTW, especially for $k_r t_{HRT} > 10$ followed by FTW position and FTW geometry.
- Positioning both the inlet and outlet on the same side of the longitudinal axis of the pond will promote a high-velocity stream path and result in poor hydraulic performance and pollutant mass removal efficiency.
- Circular FTW has superior pollutant mass removal efficiency (up to 94.8%) compared to other geometries, e.g., L-shaped, rectangular and triangular, mainly due to its capacity to enhance residence time within FTW. L-shaped geometry performed poorest in terms of pollutant mass removal due to low residence time of inflow within FTW.
- FTWs placed near the inlet coupled with optimum inlet–outlet configuration can enhance pollutant mass removal efficiency.
- A linear positive relationship exists between moment index and treatment efficiency at high removal rate ($k_r t_{HRT} > 10$). Hence, retrofitting an FTW in a stormwater pond in a way that promotes plug flow condition will lead towards better treatment efficiency.

Credit Author Statement

Md Nuruzzaman: Conceptualization, Methodology, Validation, Formal analysis, Investigation, Data curation, Writing – original draft; **A. H.M. Faisal Anwar:** Conceptualization, Resources, Supervision, Writing – review & editing; **Ranjan Sarukkalige**: Supervision, Writing – review & editing.

Declaration of competing interest

The authors declare that they have no known competing financial interests or personal relationships that could have appeared to influence the work reported in this paper.

Data availability

All data related to this article are presented within the main article and supplementary data.

Acknowledgement

This research was supported by the Australian Government Research Training Program (RTP) Scholarship for the first author at Curtin University, Western Australia. The authors would like to thank Garry Woodward and Luke Verduyn for manufacturing the experimental tank.

Appendix A. Supplementary data

Supplementary data to this article can be found online at https://doi.org/10.1016/j.jenvman.2023.117746.

References

ANSYS Inc, 2015. User's guide release 16.1. ANSYS Fluent Theory Guid 17, 0.
Bodin, H., Mietto, A., Ehde, P.M., Persson, J., Weisner, S.E.B., 2012. Tracer behaviour and analysis of hydraulics in experimental free water surface wetlands. Ecol. Eng. 49, 201–211.
Borne, K.E., Fassman, E.A., Tanner, C.C., 2013. Floating treatment wetland retrofit to improve stormwater pond performance for suspended solids, copper and zinc. Ecol. Eng. 54, 173–182.
Bu, F., Xu, X., 2013. Planted floating bed performance in treatment of eutrophic river water. Environ. Monit. Assess. 185, 6369–9651.

Chang, N.-B., Xuan, Z., Marimon, Z., Islam, K., Wanielista, M.P., 2013. Exploring hydrobiogeochemical processes of floating treatment wetlands in a subtropical stormwater wet detention pond. Ecol. Eng. 54, 66–76.
Chua, L.H.C., Tan, S.B.K., Sim, C.H., Goyal, M.K., 2012. Treatment of baseflow from an urban catchment by a floating wetland system. Ecol. Eng. 49, 170–180.
Colares, G.S., Dell'Osbel, N., Wiesel, P.G., Oliveira, G.A., Lemos, P.H.Z., da Silva, F.P., Lutterbeck, C.A., Kist, L.T., Machado, Ê.L., 2020. Floating treatment wetlands: a review and bibliometric analysis. Sci. Total Environ. 714, 136776.
Farjood, A., Melville, B.W., Shamseldin, A.Y., Adams, K.N., Khan, S., 2015. Evaluation of hydraulic performance indices for retention ponds. Water Sci. Technol. 72, 10–21.
Faulwetter, J.L., Burr, M.D., Cunningham, A.B., Stewart, F.M., Camper, A.K., Stein, O.R., 2011. Water science and technology. Floating treatment wetlands for domestic wastewater treatment 64, 2089–2095.
Faupel, F., 1992. Diffusion in non-crystalline metallic and organic media. Phys. Status Solidi 134 (1), 9–59.
Fogler, H.S., Brown, L.F., 2006. Distributions of residence times for chemical reactors. Elem. Chem. React. Eng. 4.
García, J., Solimeno, A., Zhang, L., Marois, D., Mitsch, W.J., 2020. Constructed wetlands to solve agricultural drainage pollution in South Florida: development of an advanced simulation tool for design optimization. J. Clean. Prod. 258, 120868.
Hamby, D.M., 1994. A review of techniques for parameter sensitivity analysis of environmental models. Environ. Monit. Assess. 32, 135–154.
Hartshorn, N., Marimon, Z., Xuan, Z., Cormier, J., Chang, N.-B., Wanielista, M., 2016. Complex interactions among nutrients, chlorophyll-a, and microcystins in three stormwater wet detention basins with floating treatment wetlands. Chemosphere 144, 408–419.
Headley, T.R., Tanner, C.C., 2012. Constructed wetlands with floating emergent macrophytes: an innovative stormwater treatment technology. Crit. Rev. Environ. Sci. Technol. 42, 2261–2310.
Hilton, A., Armstrong, R.A., 2006. Statnote 6: post-hoc ANOVA tests, 2006 Microbiol. 34–36.
Hoffman, F.O., Gardner, R.H., 1983. Evaluation of uncertainties in environmental radiological assessment models. Radiol. assessments a Textb. Environ. dose Assess. 11, 1.
Kadlec, R.H., Wallace, S., 2008. Treatment Wetlands. CRC press.
Khan, S., Melville, B.W., Shamseldin, A., 2013a. Design of storm-water retention ponds with floating treatment wetlands. J. Environ. Eng. 139, 1343–1349.
Khan, S., Melville, B.W., Shamseldin, A.Y., Fischer, C., 2013b. Investigation of flow patterns in storm water retention ponds using CFD. J. Environ. Eng. 139, 61–69.
Khan, S., Shoaib, M., Khan, M.M., Melville, B.W., Shamseldin, A.Y., 2019. Hydraulic investigation of the impact of retrofitting floating treatment wetlands in retention ponds. Water Sci. Technol. 80 (8), 1476–1484.
Kundu, P., Kumar, V., Mishra, I.M., 2016. Experimental and numerical investigation of fluid flow hydrodynamics in porous media: characterization of pre-Darcy, Darcy and non-Darcy flow regimes. Powder Technol. 303, 278–291.
Li, S., Katul, G., 2020. Contaminant removal efficiency of floating treatment wetlands. Environ. Res. Lett. 15, 1040b7.
Lightbody, A.F., Nepf, H.M., Bays, J.S., 2009. Modeling the hydraulic effect of transverse deep zones on the performance of short-circuiting constructed treatment wetlands. Ecol. Eng. 35, 754–768.
Liu, C., Shan, Y., Lei, J., Nepf, H., 2019. Floating treatment islands in series along a channel: the impact of island spacing on the velocity field and estimated mass removal. Adv. Water Resour. 129, 222–231.
Lucke, T., Walker, C., Beecham, S., 2019. Experimental designs of field-based constructed floating wetland studies: a review. Sci. Total Environ. 660, 199–208.
Lynch, J., Fox, L.J., Owen Jr., J.S., Sample, D.J., 2015. Evaluation of commercial floating treatment wetland technologies for nutrient remediation of stormwater. Ecol. Eng. 75, 61–69.
McAndrew, B., Ahn, C., Spooner, J., 2016. Nitrogen and sediment capture of a floating treatment wetland on an urban stormwater retention pond—the case of the rain project. Sustainability 8, 972.
McKight, P.E., Najab, J., 2010. Kruskal-wallis test. corsini Encycl. Psychol. 1.
Menter, F.R., Kuntz, M., Langtry, R., 2003. Ten years of industrial experience with the SST turbulence model. Turbul. heat mass Transf. 4, 625–632.
Nuruzzaman, M., Anwar, A.H.M.F., Sarukkalige, R., Sarker, D.C., 2021. Review of hydraulics of Floating Treatment Islands retrofitted in waterbodies receiving stormwater. Sci. Total Environ., 149526
Paul, A., Laurila, T., Vuorinen, V., Divinski, S.V., 2014. Thermodynamics, Diffusion and the Kirkendall Effect in Solids. Springer International Publishing, Cham, pp. 115–139.
Pavlineri, N., Skoulikidis, N.T., Tsihrintzis, V.A., 2017. Constructed floating wetlands: a review of research, design, operation and management aspects, and data meta-analysis. Chem. Eng. J. 308, 1120–1132.
Persson, J., Wittgren, H.B., 2003. How hydrological and hydraulic conditions affect performance of ponds. Ecol. Eng. 21, 259–269.
Plew, D.R., 2011. Depth-averaged drag coefficient for modeling flow through suspended canopies. J. Hydraul. Eng. 137 (2), 234–247.
Schmid, B.H., Hengl, M.A., 2017. Salt tracer experiments in wetland ponds: will density stratification spoil the outcome?. In: EGU General Assembly Conference Abstracts, p. 2314.
Schwammberger, P.F., Lucke, T., Walker, C., Trueman, S.J., 2019. Nutrient uptake by constructed floating wetland plants during the construction phase of an urban residential development. Sci. Total Environ. 677, 390–403.
Sonnenwald, F., Stovin, V., Guymer, I., 2016a. Feasibility of the porous zone approach to modelling vegetation in CFD. In: Hydrodynamic and Mass Transport at Freshwater Aquatic Interfaces. Springer, pp. 63–75.
Sonnenwald, F., Stovin, V., Guymer, I., 2016b. Computational fluid dynamics modelling of a vegetated stormwater pond. In: 11th International Symposium on Ecohydraulics (ISE 2016). Engineers Australia, p. 271.
Wahl, M.D., Brown, L.C., Soboyejo, A.O., Martin, J., Dong, B., 2010. Quantifying the hydraulic performance of treatment wetlands using the moment index. Ecol. Eng. 36, 1691–1699.
Wang, C.-Y., Sample, D.J., 2013. Assessing floating treatment wetlands nutrient removal performance through a first order kinetics model and statistical inference. Ecol. Eng. 61, 292–302.
Winston, R.J., Hunt, W.F., Kennedy, S.G., Merriman, L.S., Chandler, J., Brown, D., 2013. Evaluation of floating treatment wetlands as retrofits to existing stormwater retention ponds. Ecol. Eng. 54, 254–265.
Xavier, M.L.M., Janzen, J.G., Nepf, H., 2018. Numerical modeling study to compare the nutrient removal potential of different floating treatment island configurations in a stormwater pond. Ecol. Eng. 111, 78–84.
Yamasaki, T.N., Walker, C., Janzen, J.G., Nepf, H., 2022. Flow distribution and mass removal in floating treatment wetlands arranged in series and spanning the channel width. J. Hydro-environment Res. 44, 1–11.